Hindawi
Shock and Vibration
Volume 2021, Article ID 8670882, 15 pages
https://doi.org/10.1155/2021/8670882

Research Article

Influence of Cord Parameters on the Load Characteristics of Airbags

Yu-Ru Li,[1,2] **Shou-Ne Xiao**,[2] **Jun-Ke Xie**,[3] **Tao Zhu**,[2] **Bing Yang**,[2] **Guang-Wu Yang**,[2] **and Shi-De Xiao**[1]

[1]*School of Mechanical Engineering, Southwest Jiaotong University, Chengdu 610031, China*
[2]*State Key Laboratory of Traction Power, Southwest Jiaotong University, Chengdu 610031, China*
[3]*School of Mechanical Engineering, Sichuan University of Science and Engineering, Zigong 643000, China*

Correspondence should be addressed to Shou-Ne Xiao; snxiao@swjtu.cn

Received 17 May 2021; Revised 31 August 2021; Accepted 11 September 2021; Published 23 September 2021

Academic Editor: Andrea Spaggiari

Copyright © 2021 Yu-Ru Li et al. This is an open access article distributed under the Creative Commons Attribution License, which permits unrestricted use, distribution, and reproduction in any medium, provided the original work is properly cited.

To accurately characterize the large deformation and nonlinear characteristics of airbags, the influence of cord parameters on vertical force characteristics was studied, and a finite-element simulation model of airbags based on gas-solid coupling was established. First, uniaxial tension and compression experiments with airbag under different initial pressures were carried out to analyse the effects of the initial pressure and working height on the mechanical properties of the airbag. Second, the validity of the model was verified by the test data of the vertical force and cavity pressure of the airbag. Finally, based on the gas-solid coupling model proposed, the influence of the cord parameters on the vertical force characteristics was studied. The results show that the vertical force characteristics of an airbag are different between compression and tension and the nonlinear characteristic of the airbag becomes more obvious with the increase in the displacement in compression. After comparing the effects of cord parameters on the vertical force of the airbag, we can conclude that the number of cord layers has the most significant effect on the vertical force, followed by the cord diameter, while other cord parameters have a general effect. Under the same compression and tension displacements ($d = \pm 80$ mm), the effective area of 1 cord layer is 2.56 times as much as the effective area of 6 cord layers and the vertical force of the airbag with a cord diameter of 0.25 mm is 7.28 times greater than that of the corresponding vertical force with a cord diameter of 1.0 mm. The airbag with different cord angles shows differences in the working state of compression and tension, especially in compression. The force of the airbag at 90° cord angle gradually exceeds the force at other angles with an increase in displacement. The difference in the load at different working states of compression and tension is useful.

1. Introduction

Air springs are composite materials composed of cord and rubber that have strong material nonlinearity, geometric nonlinearity, and contact nonlinearity in a typical airbag. Owing to its variable stiffness, low natural frequency, and as an excellent vibration isolator, air springs have been widely used in railway vehicles, luxury buses, intercity buses, and commercial vehicles [1–5]. In addition, air springs have been applied in ejection impact and other fields and show excellent performance [6].

A series of studies have been carried out to establish an analytical model of the nonlinear characteristics of air springs. For example, Zargar et al. [7] established a nonlinear theoretical model and verified the correctness of its mathematical model through experiments. Quaglia et al. [8] theoretically deduced the expression of the stiffness of the air spring of a capsule-type revolution body and analysed the variation in the effective area in detail using the graphical method [9]. de Melo and Chang and other scholars have carried out a series of studies on the dynamic characteristics of air springs based on vehicle suspension by means of numerical analysis, model simplification, and mechanical model establishment [10, 11]. Fachinetti et al. [4] compared two modelling methods of two-stage air spring suspension and evaluated its influence on the accuracy of multibody

simulation of rail vehicle dynamics. Zhang et al. [12] proposed an air spring model with a variable orifice in an auxiliary chamber and optimized the parameters of the air spring with an auxiliary chamber, which improved the basic performance of semiactive control. Zhu et al. [13, 14] studied the nonlinear dynamic response of an air spring mechanical model under large-amplitude excitation and different precompression and pretension conditions and verified that the proposed model can predict the dynamic characteristics of an air spring through a bench test.

Some scholars apply thermodynamic theory to the air spring model to improve the calculation accuracy of the model. For example, Lee [15] established a mathematical model based on thermodynamics and believed that the stiffness of the air spring was affected by volume, heat transfer, and effective area. Okorn and Nagode [16] applied thermodynamics, heat transfer, and hydrodynamics to the model and developed a more accurate air spring suspension system model by combining these effects. Investigating the influence of an additional air chamber on the performance of an air spring, Li et al. [17] found that the shape and material characteristics of the air spring, the volume of the additional air chamber, and the diameter of the orifice are the main factors affecting the performance of the air spring. Chen et al. [18] took the air spring with orifice and additional air chamber as the research objects, established the nonlinear model, and studied the influence of the mechanical characteristics of the rubber on the dynamic characteristics of the whole air spring. Tang et al. [19] studied the influence of a single-chamber cross-section on the stiffness characteristics of membrane air spring and obtained that under the condition of determining the basic structure size, the variation of piston cone angle and piston height are the main factors affecting the single-cavity variable-section air spring.

The current research on the parameters of airbag cords focuses mainly on the modification of the tensile formula of cord rubber material parameters and the theoretical derivation of numerical models and simplified models [20–22]. Hao and Jaecheon [23] carried out a series of static and dynamic tests to measure the dynamic and static stiffness of an air spring. The research focuses mainly on the simplified model verification and dynamic characteristics of pneumatic suspension air springs. However, research on the vertical load characteristics of airbags due to changes in cord parameters is still insufficient. This paper takes the airbag as the research object, and it is effectively compounded by cord reinforcement phase and rubber matrix. The pressure load of the internal chamber is mainly carried by the cord of airbag, which has complex anisotropy and nonlinear characteristics. In this paper, the thermodynamic theory is introduced, and a simulation model of the airbag based on gas-solid coupling is established. The correctness of the model is verified based on the uniaxial tensile and compression experiment of the airbag, and on this basis, a detailed analysis is performed. The influence of cord parameters on the vertical load characteristics of the airbag is further discussed. The load characteristics of the airbag are composed mainly of vertical force, cavity pressure, cavity volume, and effective area.

2. Airbag Model

2.1. Fluid Cavity Model. The load characteristics of airbags depend not only on the geometric nonlinearity, material nonlinearity, and contact nonlinearity but also on the variation in cavity pressure. Each cavity has a unique reference point and a single degree of freedom to refer to the change in cavity pressure. The fluid element can be used to simulate various gas-filled cavities under pneumatic conditions. According to the augmented virtual work principle, the ideal gas equation is used to determine the closed gas boundary conditions, and the virtual work equation of the structure is obtained through the gas boundary conditions [14, 16, 24, 25].

Fluid volume is a function of fluid pressure, temperature, and mass. The volume of the fluid cavity $\overline{V}$ is obtained by the fluid pressure p and gas temperature θ, which is equal to the actual volume V. As the pressures of all elements in the chamber are the same, the augmented virtual work expression can be written as the sum of the expressions for individual elements. The augmented virtual work expression of the structure is realized by the following constraint equation [6, 26]:

$$\delta\Pi^* = \sum_e \left[\delta\Pi^e - p\delta V^e - \delta p\left(V^e - \overline{V}^e\right)\right], \tag{1}$$

where $\delta\Pi^*$ is the augmented virtual work expression and $\delta\Pi$ is the virtual work expression for the structure without fluid. As the temperature is the same for all elements in the cavity, the fluid volume can be calculated for each element as

$$\overline{V}^e = \overline{V}\left(p, \theta, m^e\right), \tag{2}$$

where m^e is the element mass and V can be obtained by equation (2).

$$V = \sqrt[e]{\overline{V}\left(P, \theta, m^e\right)}. \tag{3}$$

As the mass of the gas flowing into the cavity of airbag is equal to the total mass of all the fluid elements, the fluid density can be obtained as

$$p(P, \theta) = p_R \frac{\left(\theta_R - \theta_A\right)\left(P + P_A\right)}{\left(\theta - \theta_A\right)\left(P_R + P_A\right)}, \tag{4}$$

where T_R is the temperature at the reference point P_R, and the unit of temperature is K. P_R is the pressure at the reference point P_R, and the unit of pressure is Pa. θ_A is the ambient temperature, and P_A is the ambient pressure.

As all elements in the chamber have the same temperature, the fluid volume for each element is as follows:

$$\overline{V}^e = \overline{V}\left(p, \theta, m^e\right). \tag{5}$$

The volume of fluid can be expressed as

$$V = \sum_e \overline{V}^e = \sum_e \overline{V}\left(p, \theta, m^e\right) = \frac{m}{\rho(P, \theta)}. \tag{6}$$

The volume of the fluid of the flexible per pressure is

$$\frac{\mathrm{d}V}{\mathrm{d}p} = -\frac{m\mathrm{d}\rho}{\rho^2 \mathrm{d}p} = -\frac{m}{\rho_R} \frac{\left(\theta_R - \theta_A\right)\left(P + P_A\right)}{\left(\theta - \theta_A\right)\left(P_R + P_A\right)^2}. \tag{7}$$

2.2. Mechanical Model of Airbags. The ideal model of the airbag is shown in Figure 1, with the fix wall fixed and the axial force F_e acting on the move wall, and the contact area between the move wall and the airbag is A_e. Under the different pressure states on the move wall, the effective contact area between the airbag and the move wall is dynamic. P and P_a are the absolute pressure and atmospheric pressure of the chamber, respectively; T is the temperature of the chamber; F_e is the axial force along the Y direction; and V is the volume of the chamber.

The airbag allows deflection and force transmission in three directions [27]. The stiffness of the airbag was obtained based on the original ejection model, and the nonlinear stiffness of the airbag can be derived as the following equation [6]:

$$K_e = \frac{\mathrm{d}F}{\mathrm{d}x} = -\frac{nPA_e}{V}\frac{\mathrm{d}V}{\mathrm{d}x} + (P - P_a)\frac{\mathrm{d}A_e}{\mathrm{d}x}. \tag{8}$$

The temperature change in the airbag chamber is uniform, and the energy in and out of the system can be described by the first law of thermodynamics:

$$W = \Delta E + Q. \tag{9}$$

where W is the work done by the outside on the fluid in the cavity of the airbag, ΔE is the increased internal energy of the fluid in the cavity, and Q is the heat transferred from the gas in the chamber to the flexible airbag material.

The work done on the fluid can be described as

$$W = Fx - \Delta E'. \tag{10}$$

where F is the external load exerted on the airbag by the outside, x is the deformation of the airbag, and ΔE is the internal energy stored in the deformation of the airbag.

By combining equations (9) and (10), the increment of internal energy in the airbag chamber can be obtained as follows:

$$\Delta E = Fx - \Delta E' - Q. \tag{11}$$

Assuming that the fluid is an ideal gas, the relationship between temperature and energy increment is as follows:

$$\Delta E = mC_v\Delta T, \tag{12}$$

where ΔT is the temperature change in the chamber and C_v is the constant volume-specific heat of the fluid.

From equations (11) and (12), it can be concluded that

$$\Delta T = \frac{Fx - \Delta E' - Q}{mC_v}. \tag{13}$$

Q is expressed as

$$Q = \beta(T - T'). \tag{14}$$

where β is the heat transfer coefficient between the gas in the chamber and the flexible air bag, T is the fluid temperature, T' is the material temperature of the airbag, and t is the time of heat transfer.

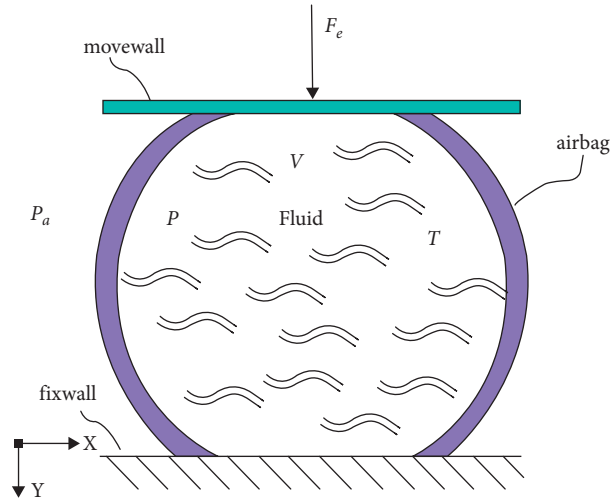

Figure 1: The airbag model.

3. Experimental Test of the Airbag

3.1. Working State Description. To study the influence of different initial pressures and working heights on the load characteristics of airbag, a uniaxial tension-compression test of airbag was carried out based on a measure testing simulation (MTS), as shown in Figure 2.

The initial working height (H) of the airbag is 300 mm, and the initial working height is defined as $d = 0$ mm. The actuator of the MTS testing machine compresses the airbag upward (the upward displacement is positive) and stretches the airbag downward (the downward displacement is negative). The maximum compression and tension displacements are +80 and −140 mm, respectively. The experimental equipment used was an MTS 809.25 testing machine, the axial load range was ±250 kN, and the accuracy of the force sensor and displacement sensor was 0.5. The measurement of pressure is realized through the installation of an intelligent pressure transmitter. The pressure measurement range is $-0.1 \sim +60$ MPa.

3.2. Experimental Methods. The working principle of the airbag compression and tensile experiment is shown in Figure 3. The experiment test system consists of an air compressor, MTS testing machine, airbag, intelligent pressure transmitter, three-way valve, intake pipe, load-displacement sensor, and air compressor. First, the airbag was fixed on the MTS testing machine by fixture, then the working height of the airbag was adjusted to 300 mm by the MTS testing machine control system. The actuator was locked at this position, and the gas was injected into the cavity of the airbag through an air compressor and air inlet pipe, and the air inlet valve was closed when the pressure reached 0.204 MPa to keep the cavity pressure stable. Finally, the compression and tensile displacement functions of the airbag were set by the MTS testing machine control system, and the speed of the actuator was 70 mm/min.

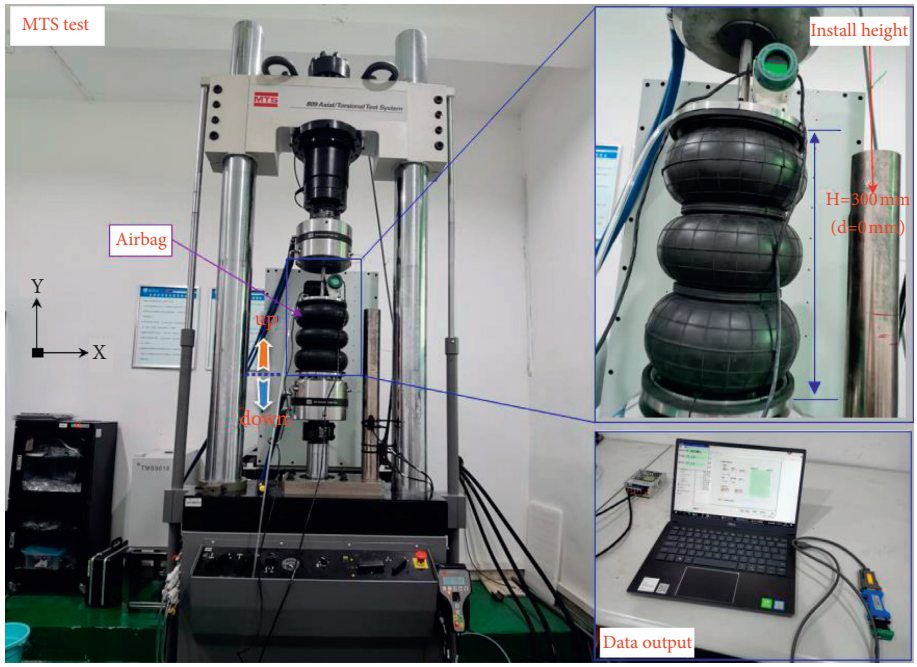

Figure 2: Tension and compression tests of the airbag.

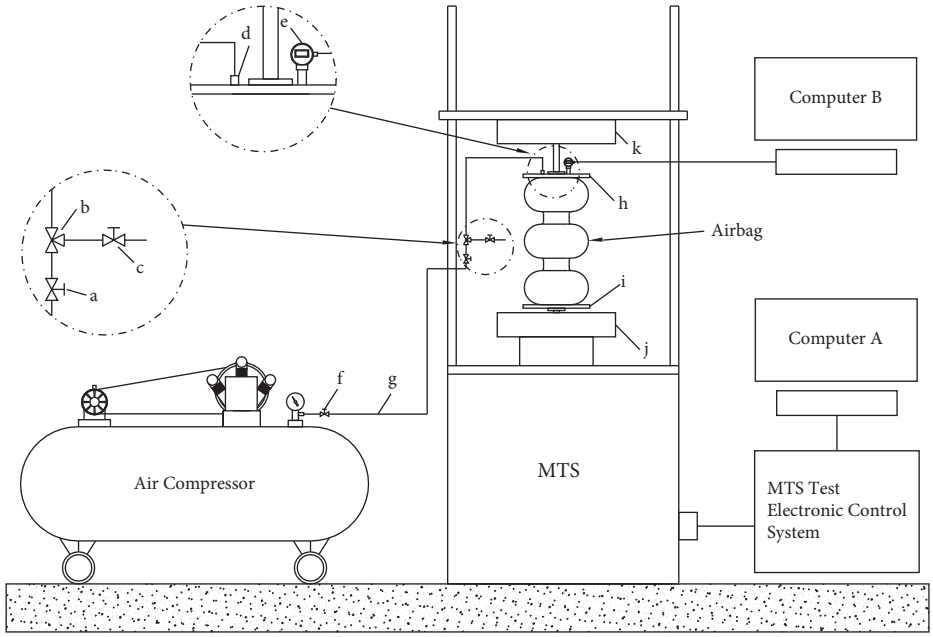

Figure 3: Tension and compression test principle of the airbag: (a) intake valve, (b) three-way valve, (c) vent valve, (d) intake port, (e) intelligent pressure transmitter, (f) intake switch, (g) intake pipe, (h) upper flange, (i) lower flange, (j) actuator, and (k) load-displacement sensor.

3.3. Experimental Results. The initial pressure (0.204, 0.408, and 0.605 MPa) was applied to the cavity of the airbag. The maximum tensile and compression displacements were −140 and + 80 mm, respectively. The changes in the vertical force and cavity pressure of the airbag with tensile and compression displacement are shown in Figure 4.

As shown in Figure 4(a), the vertical force of the airbag has obvious nonlinear characteristics with the displacement change. The larger the compression displacement, the larger the airbag load. The initial pressure has a significant effect on the nonlinearity of the vertical force. The greater the initial pressure is, the greater the stiffness of the airbag. In the

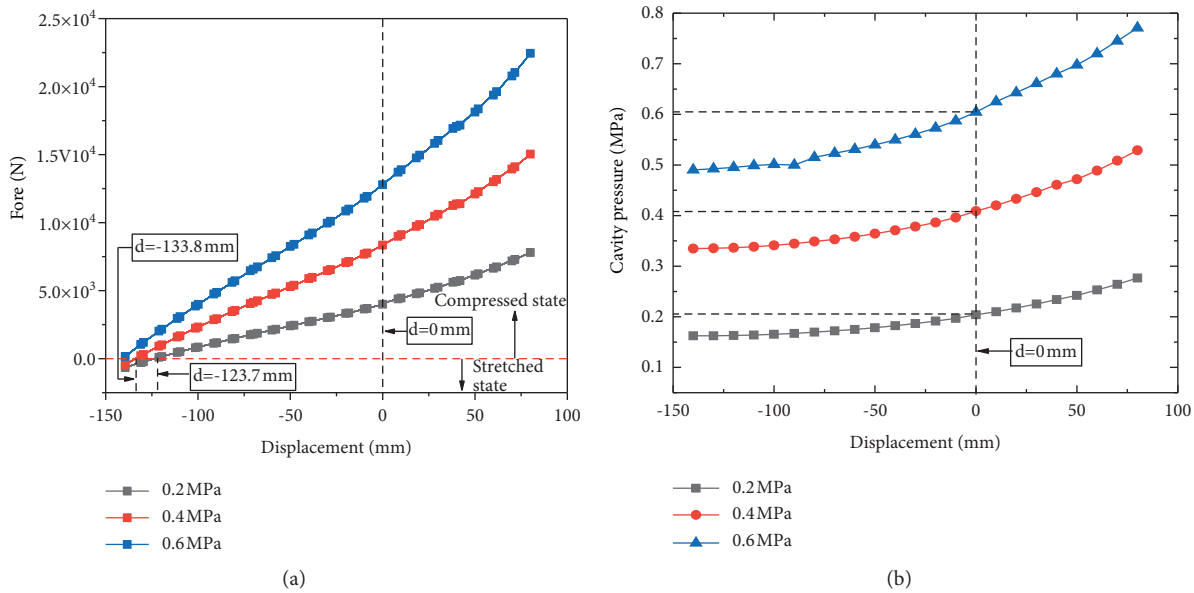

Figure 4: Uniaxial tensile and compression test results of the airbag: (a) for load change and (b) for cavity pressure change.

tensile process, with increasing tensile displacement, the load characteristics of the airbag are similar. When the tensile displacement is −123.7 mm, the airbag with an initial pressure of 0.204 MPa first changes from the compression state to the tensile state. While at 0.408 MPa, the transition displacement is −133.8 mm, and at 0.605 MPa, it changes to the tensile state at −140 mm, showing that the initial pressure has little effect on the airbag in the tensile state. However, the initial pressure has a significant effect on the airbag in the compression state. Figure 4(b) shows that with increasing compression displacement, the cavity pressure presents an obvious upward trend. The larger the compression displacement, the more obvious the nonlinearity. With increasing tensile displacement, the cavity pressure tends to maintain an approximately constant value, and the larger the tensile displacement, the more obvious the phenomenon.

The tension and compression tests were carried out on the airbag, and the variation trend of the airbag chamber temperature with the displacement under different initial pressures is discussed. The variation is shown in Figure 5.

Figure 5 shows that under the same initial pressure, the change of displacement has little effect on the temperature in the cavity of the airbag, but the overall temperature will increase with the increase of compression or tensile displacement, and the change trend under up pressure is more obvious than that under down pressure. For Figure 5(b), at the same initial displacement, the chamber temperature increases with the increase of initial pressure, from 25.8°C to 27.8°C. The results show that the initial pressure affects the chamber temperature of the airbag, while the tension displacement and compression displacement have little effect on the chamber temperature of the airbag.

4. Validation of the Airbag Simulation Model

4.1. Parameters of the Airbag Model. The Mooney–Rivlin model [28] is used to define the rubber material characteristics of the airbag. The above experiment test and analysis shows that the compression displacement and initial pressure are among the factors that affect the load characteristics of the airbag. As the airbag is a composite material with strong nonlinearity composed of a cord rubber matrix, the cords as the main load-bearing structure affect the load of the airbag. The cord distribution of the airbag rubber matrix used in the experiment is shown in Figure 6.

The cord rebar model of the airbag is shown in Figure 7 including the cord layer, cord angle, cord spacing, cord diameter, and cord centre distance. The thickness of the airbag is 6 mm, which is vulcanized by inner rubber, outer rubber, and cord, as shown in Figure 6. The cord is generally distributed symmetrically in two layers. The first cord layer is arranged in a 50° arrangement, and the second cord layer is arranged in a 50° arrangement. The cord diameter is 0.2 mm, and the cord centre distance and cord spacing are both 1 mm.

The cord layer of the airbag can be represented as a rebar element in the cord rebar model without increasing the degree of freedom, which is effective in dealing with geometric nonlinearity and physical nonlinearity [29, 30]. In the cord rebar model, the internal potential energy of cord rebar is the sum of the internal potential energy of rubber and cord.

$$\tilde{U} = \tilde{U}_1 + \tilde{U}_2, \tag{15}$$

where $\tilde{U}$ is the total internal potential energy. $\tilde{U}_1$ is the based internal potential energy. $\tilde{U}_2$ is the internal potential energy of the cord rebar.

By introducing the solid part associated with the cord to modify, and distinguishing the different functions of single cord and cord layer, the $\tilde{U}$ can be expressed as

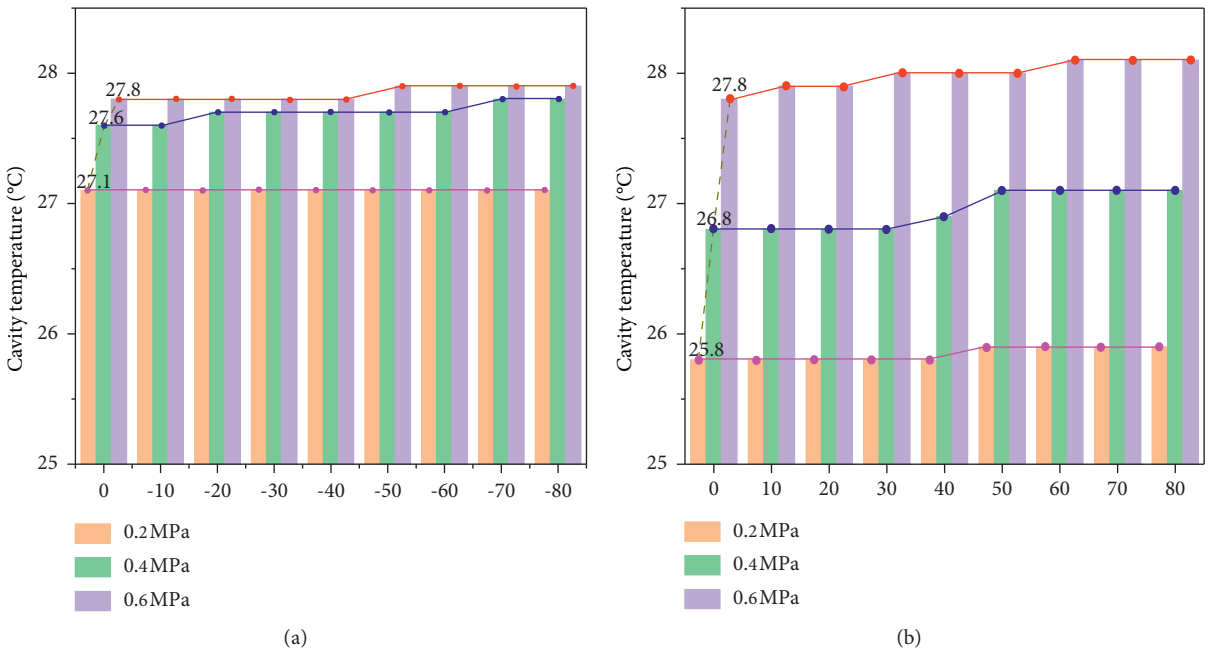

Figure 5: Airbag chamber temperature change results: (a) tension and (b) compression.

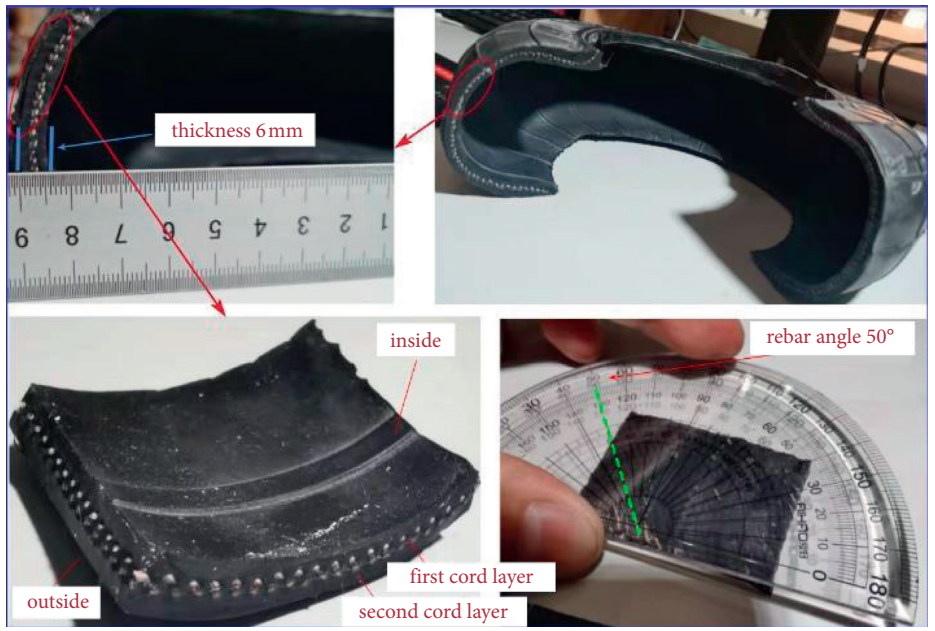

Figure 6: Cord distribution of the airbag rubber matrix.

$$\tilde{U} = \int V_e\left[W_b(\hat{E}+\tilde{E}) - S_b\colon \tilde{E}\right]\mathrm{d}V - \int V_s\left[W_b(\hat{E}+\tilde{E}) - S_b\colon \tilde{E}\right]\mathrm{d}V - \int V_r \cdot \left[W_b(\hat{E}+\tilde{E}) - S_b\colon \tilde{E}\right]\mathrm{d}V + \int\int V_s\left[W_b(\hat{E}+\tilde{E}) - S_s\colon \tilde{E}\right]V + \int V_r\left[W_b(\hat{E}+\tilde{E}) - S_r\colon \tilde{E}\right]\mathrm{d}V, \tag{16}$$

where V_e is the strain energy density of matrix material, J/m^3; $\hat{E}$ is Green Lagrange strain tensor; $\tilde{E}$ is the enhanced strain tensor; S_b is the fundamental stress tensor; W_s is strain energy density of single cord, J/m^3; W_r is the strain energy density of cord layer, J/m^3; S_r is the stress tensor of cord layer, Pa; S_s is the single-cord stress tensor, Pa; V_e is the element volume, m^3; V_s is the volume of single cord, m^3; and V_r is the volume of cord layer, m^3.

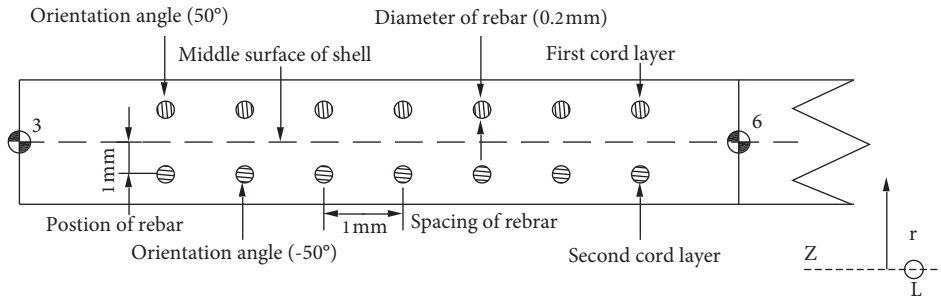

Figure 7: The cord rebar model of the airbag.

4.2. Finite-Element Simulation Model. The S4R element is used to establish the airbag simulation model with an element size of 4 mm. The number of elements is 36,034, and the number of nodes is 36,037, including the reference points of the cavity. The thickness of airbag is shown in Figure 7. The airbag was inflated with gas until the total (absolute) pressure reached 0.204 MPa. When the specified pressure was reached, the gas flowing into the airbag chamber was stopped, and the airbag was compressed upward by 80 mm. The finite-element simulation model and constraint load of the airbag are shown in Figure 8. The finite-element simulation model is a three-dimensional solid model and the geometric structure of the airbag is axisymmetric. So, the reference point of fluid cavity coincides with the center of symmetry of airbag. The end of the airbag is fully constrained, and the displacement load along the *Y*-direction is set at the other end.

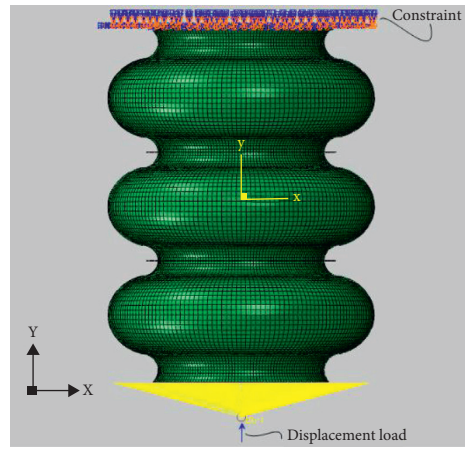

Figure 8: Finite-element model and restraint load of the airbag.

4.3. Model Validation. Based on the gas-solid coupling airbag simulation model, the changes in the vertical force and cavity pressure with the working height under different initial pressures (0.204, 0.408, and 0.605 MPa) were calculated. Different from the explicit algorithm used in the dynamic ejection model, the implicit algorithm is used in the quasi-static calculation of airbag. The simulation results (Sim) compared with the experimental data (Exp) are shown in Figure 9.

The comparison results in Figure 9 show that the variation of cavity pressure obtained by simulation calculation is close to the experimental value, and the variation trend is the same. Since the force is related to not only the cavity pressure but also the effective contact area of the airbag, there is a certain error in the simulation calculation of the load, but within the acceptable range. With increasing compression displacement, the vertical force and cavity pressure also change nonlinearly. The simulation results are close to the experimental results, and the experimental results verify the correctness of the finite-element simulation model.

Based on the simulation model verification, the influence of cord parameters on the vertical force, cavity pressure, cavity volume, and effective area of the airbag were investigated. The following research on cord parameters is based on an initial pressure of 0.204 MPa and a displacement of 80 mm in compression and tensile testing.

5. Results and Discussion

5.1. Influence of Different Cord Layers on the Characteristics of Airbags. The cord layer of the airbag is usually arranged in two layers. Based on the established finite-element simulation model of a gas-solid coupling airbag, the distribution of different cord layers was investigated. The influence of cord layers on the vertical force, cavity pressure, cavity volume, and effective area is obtained, as shown in Figure 10.

As Figure 10(a) shows, the vertical force of the airbag increases with the increase in the number of cord layers in both the compression and tensile states and is significantly increased, which indicates that the vertical force can be significantly improved by increasing the number of cord layers. For the airbag with 1 and 2 cord layers, the force difference is small when the airbag is compressed, while the force difference is obvious in tensile testing, indicating that the force characteristics are not completely consistent when the cord has only one or two layers, and there are differences.

Figure 10(b) shows that the cavity pressure increases with increasing compression displacement. The effect of cord layers on cavity pressure becomes obvious with increasing displacement when the airbag is in compression. When stretching, the airbag was stretched by the actuator, the effect of cord layers on cavity pressure is very small, and the cavity pressure of different cord layers remains the same. With increasing tensile displacement, the cavity pressure gradually decreases. For the pressure change trend, when the

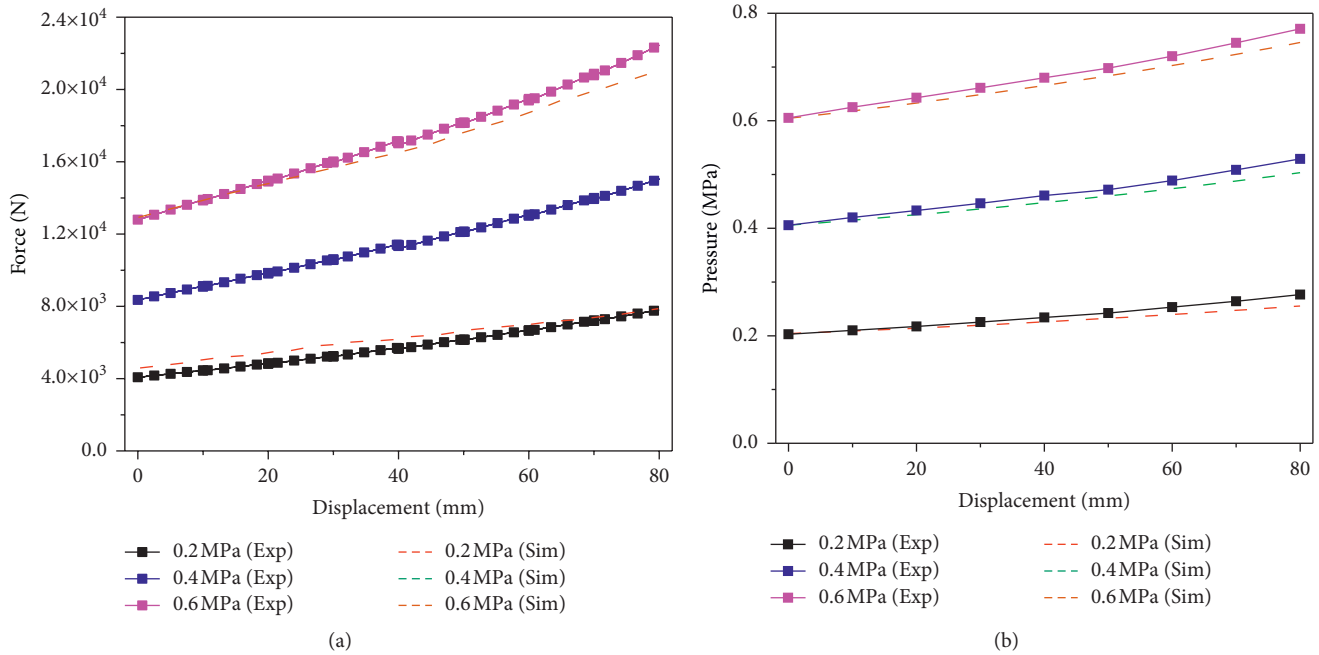

Figure 9: Experimental simulation results: (a) for force and (b) for pressure.

tensile displacement reaches a certain value, the final cavity pressure will tend to a constant value. This shows that the initial tensile displacement has a significant effect on the cavity pressure, but when the tensile displacement is large, the pressure will not change.

For the change in cavity volume in Figure 10(c), the volume decreases with increasing compression displacement and increases with increasing tensile displacement. At the same working height, with the increase in the number of cord layers, the cavity volume of the airbag will decrease, while the extent of reduction will decrease with the increase in the number of cord layers. After reaching a certain number of cord layers, the cavity volume will remain the same, and the change in the number of cord layers will have no influence on the volume.

The change trend in the effective area in Figure 10(d) is consistent with the change trend in the force. The effective area increases with the increase in the number of cord layers, regardless of compression or tensile. At the same compression and tensile displacement ($d = +80$ mm and $d = -80$ mm), the effective area difference of the 1 cord layer and 6 cord layers is 35,143 and 13,705 mm^2, respectively. The difference of 2.56 times indicates that the number of cord layers has a significant effect on the effective area, which shows that the effect of the cord layer number on the effective area when the airbag is in the tensile is much greater than the compression.

5.2. Influence of Cord Layer Spacing on the Characteristics of the Airbag. The cord layer spacings of the airbag are 1.5, 2.0, 2.5, and 3.0 mm. When the initial pressure is 0.204 MPa and the compression and tensile displacement are both 80 mm, the influence of cord layer spacing on the vertical force, cavity pressure, cavity volume, and effective contact area was studied. The calculation result based on the finite-element simulation model of a gas-solid coupling airbag is shown in Figure 11.

Figure 11(a) shows that the vertical force decreases with increasing cord spacing. Especially when the airbag was stretched by the actuator, the difference in the vertical force was more obvious. The difference in vertical force is very small when the airbag is in the compression, indicating that the cord spacing has a significant effect on the vertical force when airbag is in the tension.

As shown in Figure 11(b), the cavity pressure of the airbag is almost the same at the different cord spacings, regardless of whether the airbag is in the compression or tensile, showing that the cord spacing has little effect on the cavity pressure.

For the change in cavity volume under different cord spacings in Figure 11(c), the cavity volume increases with increasing cord spacing at the same working height, but the increase is small. The cavity volume does not change because the airbag is in the compression and tension states.

Figure 11(d) shows that the change trend of the effective area of the airbag is consistent with the change in the load, and the effective area is different when the airbag is compressed and stretched. The effective area decreases with increasing cord spacing in the tensile state, showing that the vertical force difference with different cord spacings is caused mainly by the change in effective area.

5.3. Influence of Cord Diameter on the Characteristics of Airbags. The influence of cord diameter on the vertical force characteristics of airbag was investigated by changing the

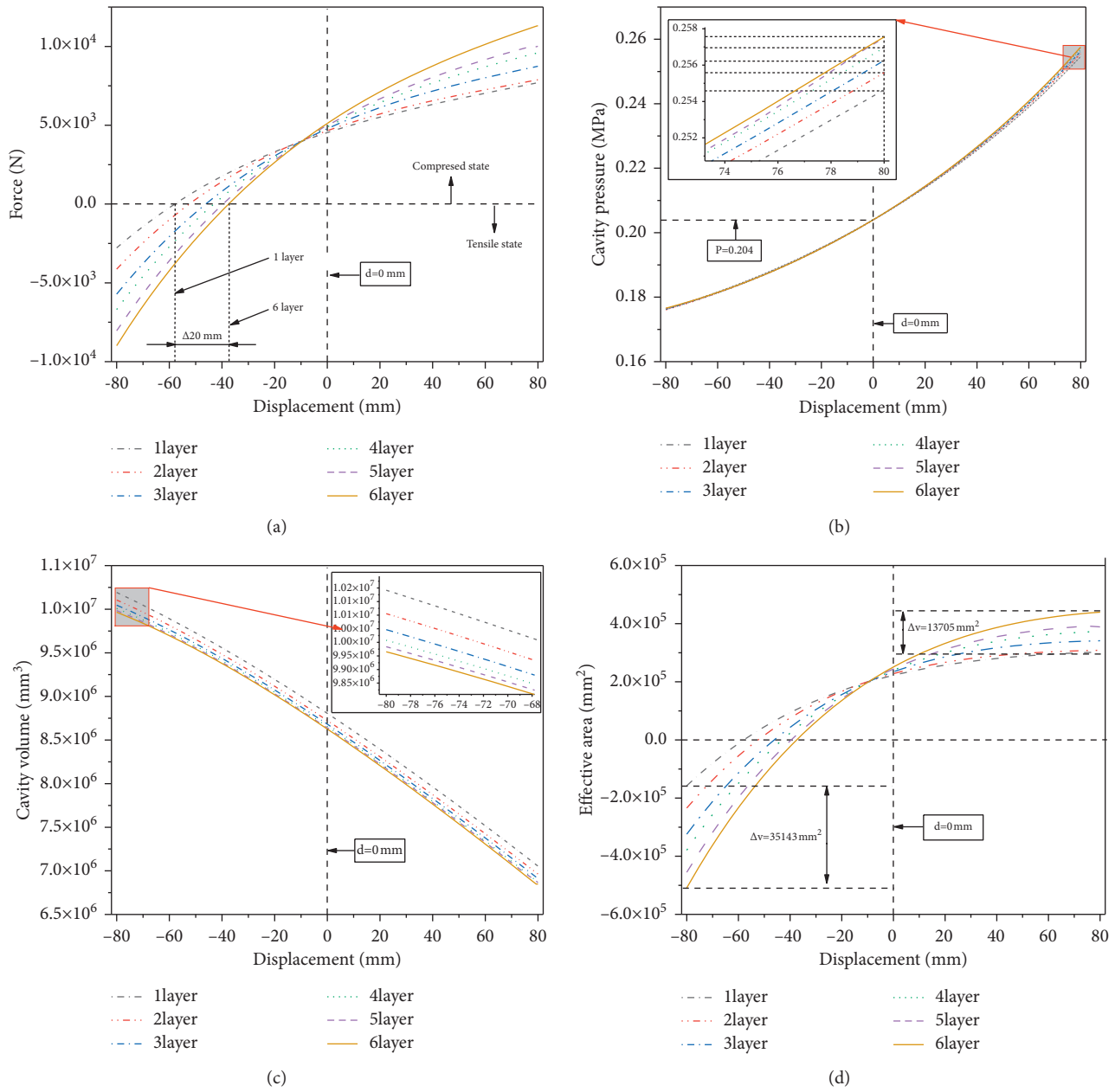

Figure 10: The results of the investigation of the influence of the cord layer on the airbag: (a) for the load, (b) for the pressure, (c) for the volume, and (d) for the effective area.

cord diameter (0.25, 0.5, 0.75, and 1.0 mm). The result is shown in Figure 12.

As shown in Figure 12(a), the vertical force of the airbag increases with increasing cord diameter regardless of compression or tensile testing. Especially when it is tensile, the cord diameter has a more obvious effect on the vertical force of the airbag. When the tensile displacement is −80 mm, the vertical force difference of the airbag corresponding to cord diameters of 0.25 mm and 1.0 mm is 3029 N, which is 7.28 times the vertical force difference when the compression displacement is 80 mm, showing that the cord diameter is more sensitive to the vertical force of the airbag in the tensile test.

Figure 12(b) shows that the cavity pressure of airbag with different cord diameters increases with increasing displacement under compression. However, the cavity pressure decreases with increasing displacement when it is tensile. In compression, the cavity pressure increases with increasing cord diameter. In the tensile test, the cord diameter has little effect on the cavity pressure. When the cord diameter is greater than 0.25 mm, the load values of different cord diameters are similar, and there is no increase with increasing cord diameter.

Figure 12(c) shows that under different cord diameters, the volume of the airbag chamber decreases with increasing compression displacement. Under the same displacement,

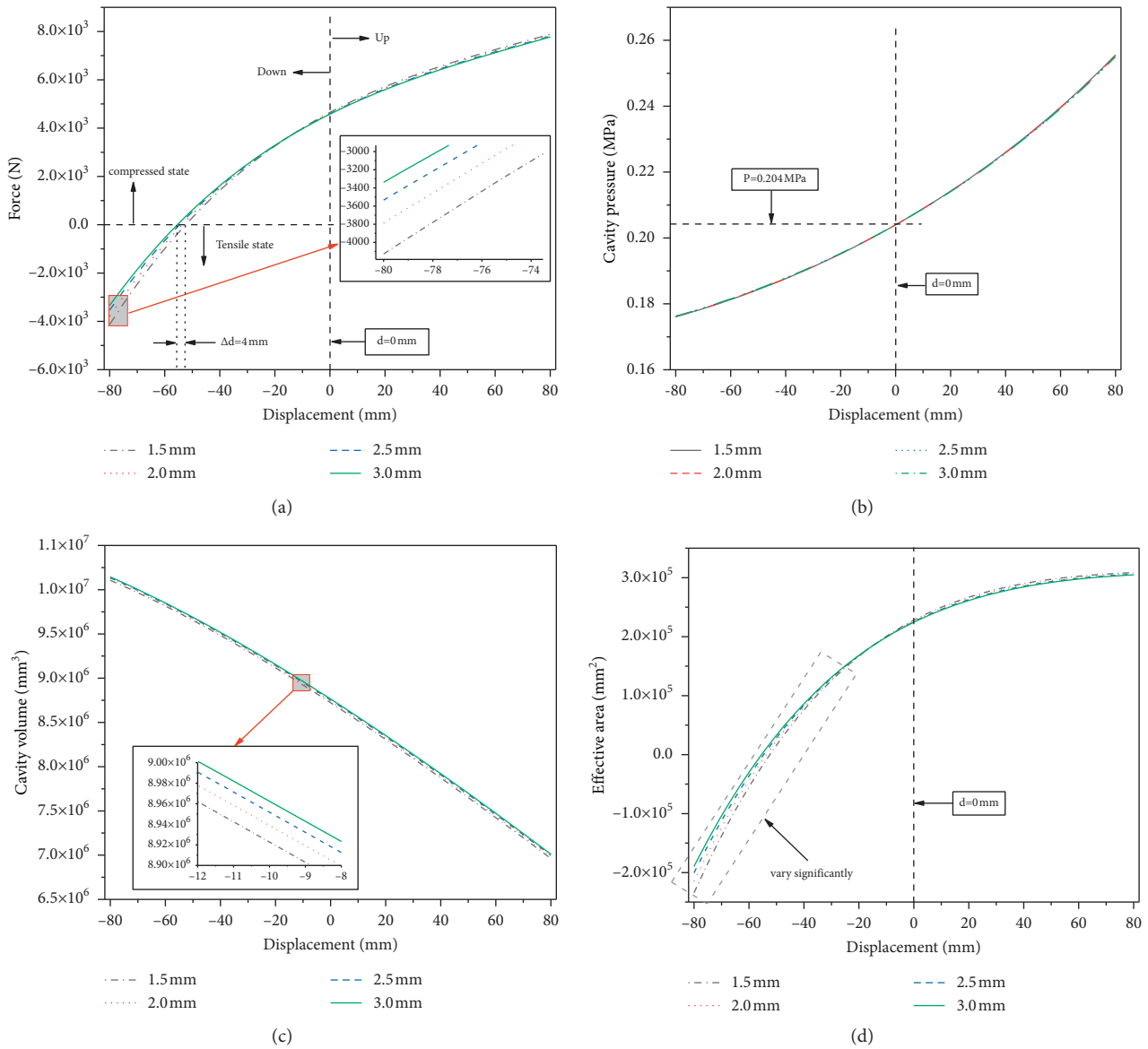

Figure 11: Effect of cord layer spacing on airbags: (a) for load, (b) for pressure, (c) for volume, and (d) for effective area.

the volume of the airbag chamber decreases with increasing cord diameter, but the reduction amplitude decreases. When the cord diameter reaches 0.75 mm or above, the volumes of the airbag chamber are close to each other.

Figure 13(d) shows the variation in the effective area of the airbag with different values. When it is pulled down, the effective area of the airbag increases with increasing cord diameter. The difference in effective area between the 0.25 mm cord diameter and 1.0 mm cord diameter is 17,223 and 2589 mm, respectively. The effective area is 6.65 times different. Especially from tensile to compression, the effective area of the airbag changes through two different phases. In Phase 1, with increasing compression displacement, the effective area difference of airbag with different cord diameters increases. However, in Phase 2, when the compression displacement is greater than 33.3 mm, the effective area difference of airbag with different cord diameters decreases significantly.

5.4. Influence of Cord Angle on the Characteristics of Airbags. The cord angles were 10°, 20°, 30°, 40°, 50°, 60°, 70°, 80°, and 90°. The effects of the vertical force, cavity pressure, cavity volume, and effective area of the airbag were studied by changing the cord angle. The results are shown in Figure 13.

Figure 13(a) shows that the vertical force of the airbag has obvious differences in compression and tensile strength. In the tensile test, the vertical force has the maximum tensile load when the cord angle is 20°. When the cord angle is 90° and the compression displacement is 80 mm, the vertical force reaches its maximum, which indicates that the cord angle has a significant difference at different working heights. However, the change of cord angle has little

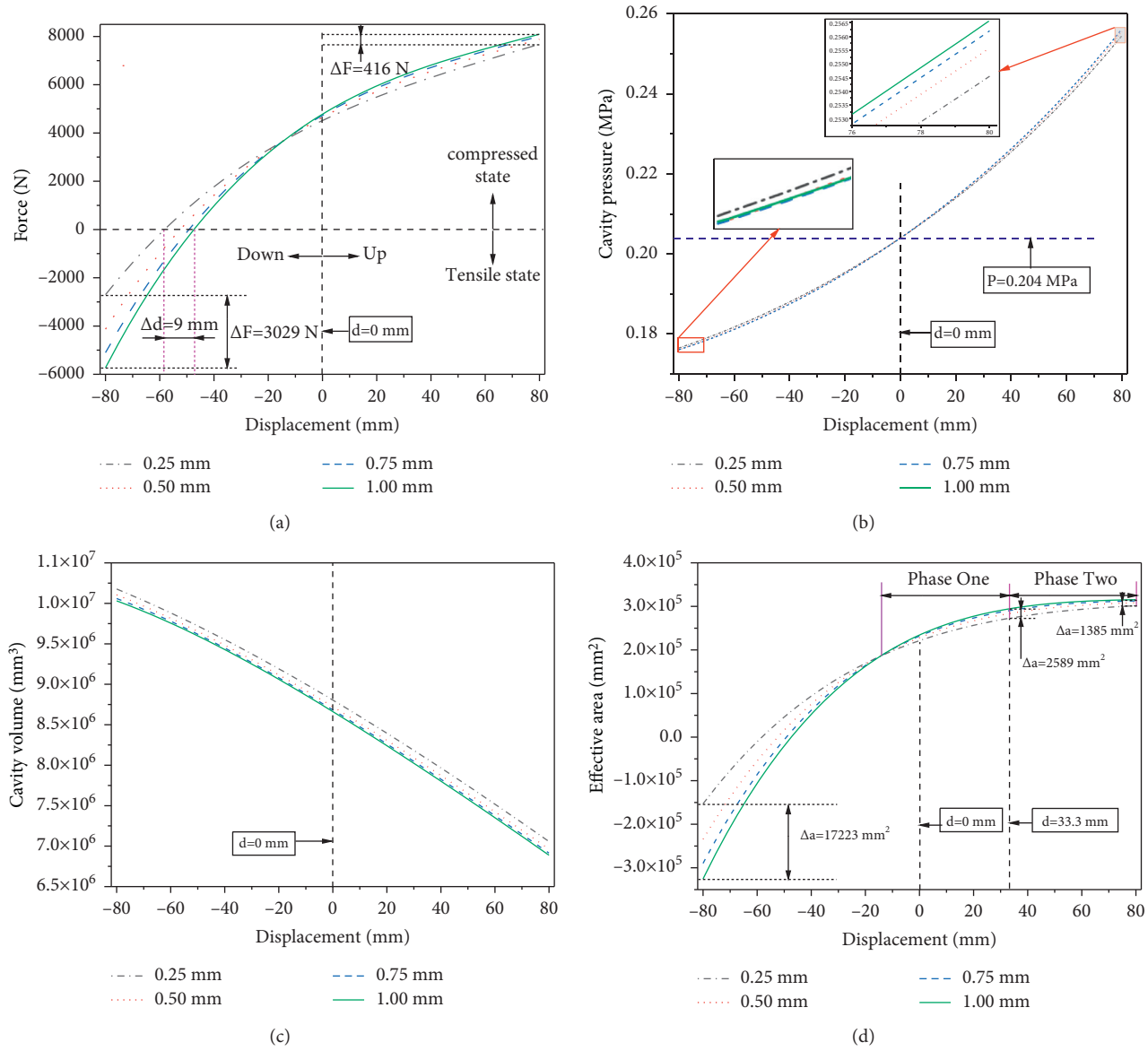

Figure 12: Effect of cord diameter on airbag: (a) for load, (b) for pressure, (c) for volume, and (d) for effective area.

influence on the dynamic ejection velocity of the airbag [6]. Different from dynamic ejection, the airbag under static load shows obvious differences, which is of great significance to the application of airbags under different states.

Figure 13(b) shows that different cord angles have a certain influence on the cavity pressure of the airbag, especially when the cord angle is 20°. The cavity pressure is the lowest, and when the cord angle is 90°, the cavity pressure is the highest. When $d < 0$, the effect of the cord angle on the cavity pressure becomes increasingly obvious with increasing tensile displacement.

As shown in Figure 13(c), the cavity volume decreases with increasing compression displacement, and the cavity volume of the airbag has different variation rules under different cord angles. When the tensile displacement is more than 30 mm, the cavity volume of the airbag at the cord angle of 30° and below obviously begins to change. Finally, with the increase in the displacement, the cavity volume is larger than the cavity volume at other angles, which is also the main reason for the decrease in the cavity pressure of the airbag at cord angles of 30° and below.

Figure 13(d) shows that the effective area of the airbag has certain differences under different compression and tensile stresses. When the airbag is tensile, the effective area is the largest when the cord angle is 20°. However, in compression, with increasing compression displacement, the effective area of the airbag with cord angles of 90°, 80°, and 70° gradually exceeds the effective area at other angles.

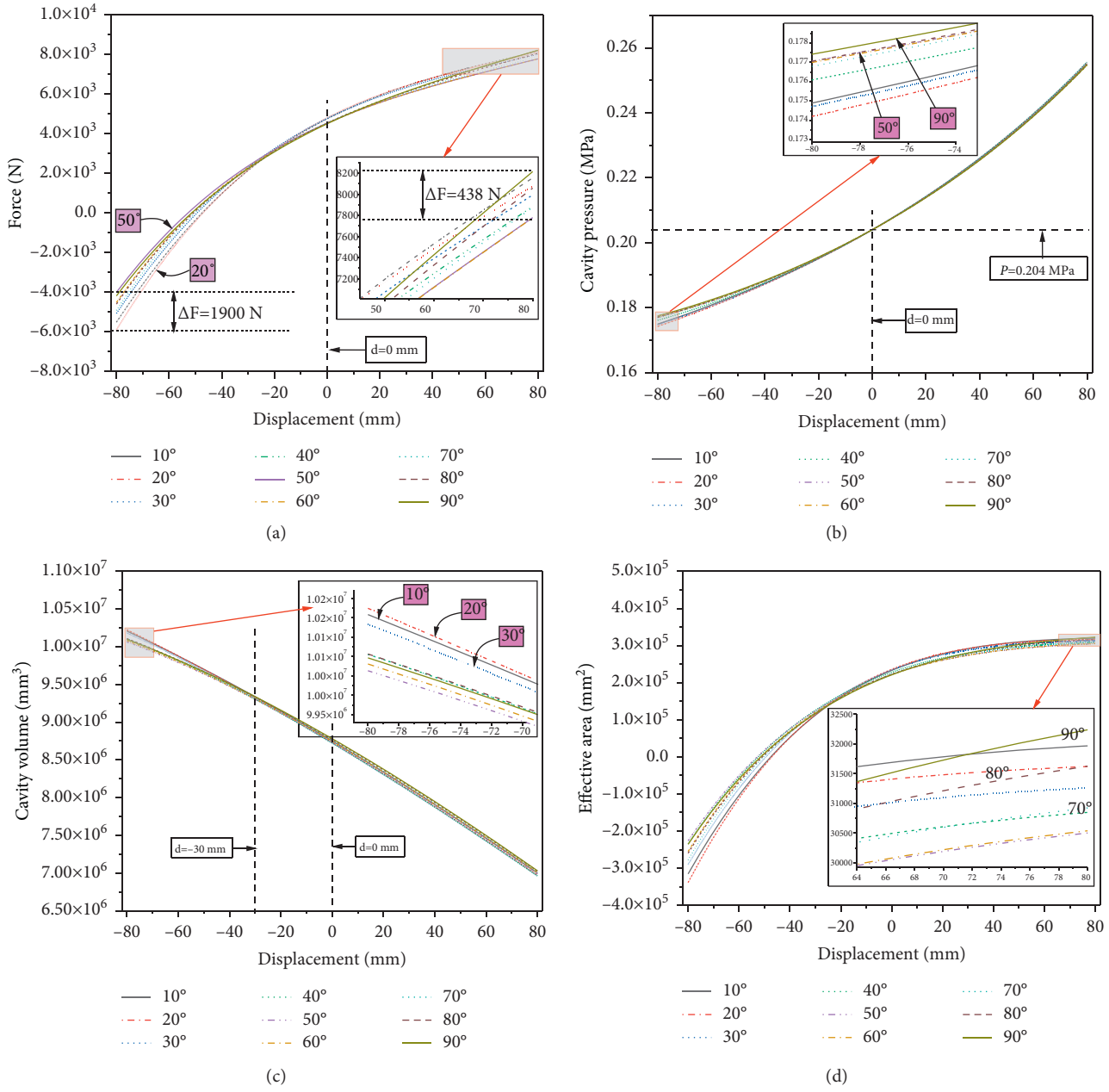

Figure 13: Effect of cord angle on airbag: (a) for load, (b) for pressure, (c) for volume, and (d)for effective area.

5.5. Influence of Centre Distance on the Characteristics of Airbags. The centre distances of the cord are 1.0, 1.5, 2.0, and 2.5 mm. By changing the centre distance, the change rules of the force, cavity pressure, cavity volume, and effective area of the airbag were studied, and the results are shown in Figure 14.

Figures 14(a) and 14(d) shows that the vertical force and effective area of the airbag increase with increasing centre distance when it is in compression, but there is no obvious difference in the change in the vertical force and effective area for the tensile airbag. Figures 14(b) and 14(c) show that different cord centre distances have almost no effect on the cavity pressure and cavity volume, which increase with increasing compression displacement and decrease with increasing tensile displacement, with almost the same change value.

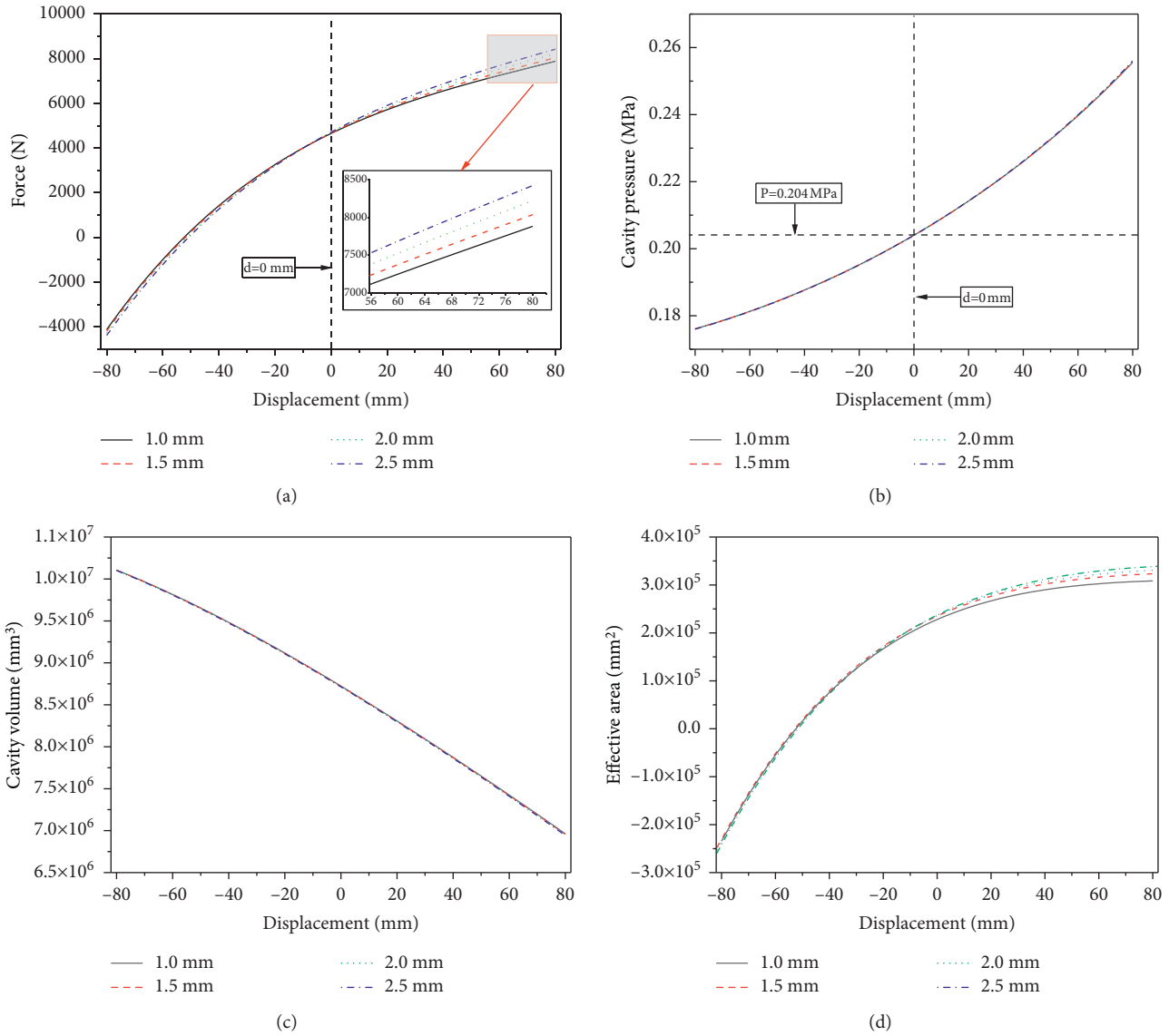

Figure 14: Effect of centre distance on the airbag: (a) force, (b) pressure, (c) volume, and (d) effective area.

6. Conclusion

Based on the MTS testing machine, a uniaxial tensile-compression experimental test of the airbag was performed. The vertical force nonlinearity of the airbag became more obvious with increasing displacement when the airbag was in compression. The vertical force of the airbag at different initial pressures tended to be gradually consistent when in tensile testing. Finally, the airbag changed from the state of compression to the tensile state with increasing tensile displacement, and the airbag with the lowest initial pressure first reached the tensile state. In the tensile state, different initial pressures tended to a constant value and no longer changed with increasing tensile displacement.

Based on the finite-element model proposed, the effect of cord parameters on airbag was studied. The comparison results showed that the number of cord layers and cord diameter have obvious influences on the load characteristics of airbag, while the cord angle, cord spacing, and cord centre distance have less influence, among which the cord layer has the most significant influence. In addition, the more cord layers there are, the greater the vertical force, due mainly to the increase in the cord layers leading to the effective area of the airbag.

The results show that the cord layer spacing has a significant effect on the vertical force of the airbag in the tensile state, but the cord layer spacing has little effect on the compression. Therefore, the vertical force of the airbag can be improved by increasing the cord layer spacing. The vertical forces of the airbag at different cord angles are different, which shows differences in the tensile state and the state of compression. The cord centre distance has a significant effect on the vertical force in the state of compression, but it has little effect in the tensile state.

Data Availability

The data sets supporting the conclusion of this article are included within the article.

Conflicts of Interest

The authors declare that they have no conflicts of interest.

Acknowledgments

This research was supported by the National Natural Science Foundation Project (grant no. 52175123), Sichuan Science and Technology Foundation Project (grant nos. 2020JDRC0080 and 2019YJ0216), and Science and Technology Research and Development Program of China Railway Group Co. Ltd. (grant no. P2020J024).

References

[1] S. Bruni, J. Vinolas, M. Berg, O. Polach, and S. Stichel, "Modelling of suspension components in a rail vehicle dynamics context," *Vehicle System Dynamics*, vol. 49, no. 7, pp. 1021–1072, 2011.

[2] M. B. Kuren and A. Shukla, "System design for isolation of a neonatal transport unit using passive and semi active control strategies," *Journal of Sound and Vibration*, vol. 286, no. 1, pp. 382–394, 2005.

[3] M. W. Holtz and J. L. van Niekerk, "Modelling and design of a novel air-spring for a suspension seat," *Journal of Sound and Vibration*, vol. 329, no. 21, pp. 4354–4366, 2010.

[4] A. Facchinetti, L. Mazzola, S. Alfi, S. Alfi, and S. Bruni, "Mathematical modelling of the secondary air spring suspension in railway vehicles and its effect on safety and ride comfort," *Vehicle System Dynamics*, vol. 48, no. S1, pp. 429–449, 2010.

[5] I. Maciejewski, "Control system design of active seat suspensions," *Journal of Sound and Vibration*, vol. 331, no. 6, pp. 1291–1309, 2012.

[6] Y. R. Li, B. Yang, and J. K. Xie, "Study of influence factors on ejection impact performance of air spring," *Journal of Mechanical Engineering*, vol. 56, no. 10, pp. 144–153, 2020.

[7] B. Zargar, A. Fahim, and A. Jnifene, "Development, validation, and parameter sensitivity analyses of a nonlinear mathematical model of air springs," *Journal of Vibration and Control*, vol. 18, no. 12, pp. 1777–1787, 2011.

[8] G. Quaglia and A. Guala, "Evaluation and validation of an air spring analytical model," *International Journal of Fluid Power*, vol. 4, no. 2, pp. 43–54, 2003.

[9] G. Quaglia and M. Sorli, "Air suspension dimensionless analysis and design procedure," *Vehicle System Dynamics*, vol. 35, no. 6, pp. 443–475, 2001.

[10] F. de Melo, A. Pereira, and A. Morais, "The simulation of an automotive air spring suspension using a pseudo-dynamic procedure," *Applied Sciences*, vol. 8, no. 7, p. 1049, 2018.

[11] F. Chang and Z. H. Lu, "Dynamic model of an air spring and integration into a vehicle dynamics model," *Proceedings of the Institution of Mechanical Engineers - Part D: Journal of Automobile Engineering*, vol. 222, no. 10, pp. 1713–1825, 2008.

[12] Z. Zhang, J. Wang, W. Wu, and C. Huang, "Semi-active control of air suspension with auxiliary chamber subject to parameter uncertainties and time-delay," *International Journal of Robust and Nonlinear Control*, vol. 30, no. 17, pp. 7130–7149, 2020.

[13] H. J. Zhu, J. Yang, Y. Q. Zhang, X. Feng, and Z. Ma, "Nonlinear dynamic model of air spring with a damper for vehicle ride comfort," *Nonlinear Dynamics*, vol. 89, no. 2, pp. 1545–1568, 2017.

[14] H. Zhu, J. Yang, Y. Zhang, and X. Feng, "A novel air spring dynamic model with pneumatic thermodynamics, effective friction and viscoelastic damping," *Journal of Sound and Vibration*, vol. 408, pp. 87–104, 2017.

[15] S. J. Lee, "Development and analysis of an air spring model," *International Journal of Automotive Technology*, vol. 11, no. 4, pp. 471–479, 2010.

[16] I. Okorn and M. Nagode, "Analysis of energy efficiency of a test rig for air springs," *Strojniski Vestnik - Journal of Mechanical Engineering*, vol. 61, no. 1, pp. 53–62, 2015.

[17] F. Li, M. H. Fu, and Y. H. Huang, "Analysis of dynamic characteristic parameter of air spring," *Journal of Southwet Jiaotong University*, vol. 38, no. 3, pp. 276–281, 2003.

[18] J. J. Chen, Z. H. Yin, J. H. He, and W. B. Shangguan, "Study on modelling and dynamic characteristic of air spring with throttling damping orifice and auxiliary chamber," *Journal of Mechanical Engineering*, vol. 53, no. 8, pp. 166–174, 2017.

[19] C. Y. Tang, Y. M. Zhang, and Y. G. Li, "Analysis of stiffness characteristics and influencing factors based on single chamber cross-section air spring," *Journal of Mechanical Engineering*, vol. 50, no. 24, pp. 137–144, 2014.

[20] J. Ren and J. L. Zhong, "The accurate prediction method of tension modulus for nylon cord/rubber composite material," *Applied Mechanics and Materials*, vol. 575, pp. 115–120, 2014.

[21] V. A. Levin, K. M. Zingerman, A. V. Vershinin, and M. Y. Yakovlev, "Numerical analysis of effective mechanical properties of rubber-cord composites under finite strains," *Composite Structures*, vol. 131, pp. 25–36, 2015.

[22] C. Y. Yuan, K. K. Zhou, and L. Q. Wu, "Structural analysis method of automotive air-spring rubber air-bag," *Journal of Mechanical Engineering*, vol. 45, no. 9, pp. 221–225, 2009.

[23] L. Hao and L. Jaecheon, "Model development of automotive air spring based on experimental research," in *Proceedings of the Third International Conference on Measuring Technology and Mechatronics Automation*, pp. 585–590, Shanghai, People's Republic of China, Shangshai, China, January 2011.

[24] R. Dijk, F. Keuelen, and J. C. Sterk, "Simulation of closed thin-walled structures partially filled with fluid," *International Journal of Solids and Structures*, vol. 37, no. 42, pp. 6063–6083, 2000.

[25] Y. Xue, J. Liu, P. G. Ranjith, X. Liang, and S. Wang, "Investigation of the influence of gas fracturing on fracturing characteristics of coal mass and gas extraction efficiency based on a multi-physical field model," *Journal of Petroleum Science and Engineering*, vol. 206, Article ID 109018, 2021.

[26] S. S. Hiremath and M. Singaperumal, "Investigations on actuator dynamics through theoretical and finite element approach," *Mathematical Problems in Engineering*, vol. 2010, Article ID 191898, 2010.

[27] A. Alonso, J. G. Gimenez, J. Nieto, and J. Vinolas, "Air suspension characterisation and effectiveness of a variable area orifice," *Vehicle System Dynamics*, vol. 48, no. S1, pp. 271–286, 2010.

[28] R. S. Rivin, "Large elastic deformation of isotropic materials: I. Fundamental concepts, II. some uniqueness theorems for pure homogeneous," *Philosophical Transactions of the Royal*

Society A: Mathematical, Physical and Engineering Sciences, vol. 240, pp. 459–508, 1948.

[29] W. Sprenger and W. Wager, "On the formulation of geometrically nonlinear 3D-Rebar -elements using the enhanced assumed strain method," *Engineering Structures*, vol. 21, no. 3, pp. 209–218, 1999.

[30] G. Meschike and P. Helnwein, "Large-strain 3D analysis of fiber-rein forced composites using Rebar element: hyperelastic formulation for cord," *Computational Mechanics*, vol. 13, no. 4, pp. 241–254, 1994.